



# Operating principle of Soft Open Points for electrical distribution network operation



Wanyu Cao<sup>a</sup>, Jianzhong Wu<sup>a,\*</sup>, Nick Jenkins<sup>a</sup>, Chengshan Wang<sup>b</sup>, Timothy Green<sup>c</sup>

<sup>a</sup> Institute of Energy, School of Engineering, Cardiff University, Cardiff CF24 3AA, UK

<sup>b</sup> Key Laboratory of Smart Grid of Ministry of Education, Tianjin University, Tianjin 300072, China

<sup>c</sup> Department of Electrical and Electronic Engineering, Imperial College London, London, UK

## HIGHLIGHTS

- Two control modes were developed for a B2B VSCs based SOP.
- The SOP operating principle was investigated under various network conditions.
- The performance of the SOP using two control modes was analyzed.

## ARTICLE INFO

### Article history:

Received 31 August 2015

Received in revised form 19 November 2015

Accepted 3 December 2015

Available online 21 December 2015

### Keywords:

Soft Open Point  
Back-to-back converter  
Distribution network  
Network operation

## ABSTRACT

Soft Open Points (SOPs) are power electronic devices installed in place of normally-open points in electrical power distribution networks. They are able to provide active power flow control, reactive power compensation and voltage regulation under normal network operating conditions, as well as fast fault isolation and supply restoration under abnormal conditions. Two control modes were developed for the operation of an SOP, using back-to-back voltage-source converters (VSCs). A power flow control mode with current control provides independent control of real and reactive power. A supply restoration mode with a voltage controller enables power supply to isolated loads due to network faults. The operating principle of the back-to-back VSCs based SOP was investigated under both normal and abnormal network operating conditions. Studies on a two-feeder medium-voltage distribution network showed the performance of the SOP under different network-operating conditions: normal, during a fault and post-fault supply restoration. During the change of network operating conditions, a mode switch method based on the phase locked loop controller was used to achieve the transitions between the two control modes. Hard transitions by a direct mode switching were noticed unfavourable, but seamless transitions were obtained by deploying a soft cold load pickup and voltage synchronization process.

© 2015 The Authors. Published by Elsevier Ltd. This is an open access article under the CC BY license (<http://creativecommons.org/licenses/by/4.0/>).

## 1. Introduction

The widespread use of distributed energy resources, e.g., distributed generations (DG), energy storage and controllable loads, is anticipated in many countries but this can lead to operation problems including excessive fault level as well as violations of thermal and voltage limits [1,2]. In the UK, with the liberalization of the electricity market and the drive to reduce the number of long term interruptions of electricity supply, reliable and high quality power supply is becoming more vital than ever [3]. These

drivers inevitably lead to new challenges in the operation of electrical power distribution networks.

Medium voltage (MV) distribution networks are usually operated in a radial configuration. Normally open points (NOPs) are built, connecting adjacent feeders, to provide alternative routes of electricity supply in case of planned or unplanned power outages [4]. Such network configuration allows the use of simple and inexpensive protection schemes as well as providing fast fault isolation to limit the propagation of network faults. However, there is a possibility of power flow being unbalanced between radial feeders due to different loading conditions, especially when a high penetration of intermittent DG and flexible demand presents in the distribution networks. This, in turn, leads to high power losses, increased peak currents and undesirable voltage excursions [5]. Moreover, even though there are many supply restoration

\* Corresponding author.

E-mail addresses: [CaoW5@Cardiff.ac.uk](mailto:CaoW5@Cardiff.ac.uk) (W. Cao), [Wuj5@cardiff.ac.uk](mailto:Wuj5@cardiff.ac.uk) (J. Wu), [JenkinsN6@cardiff.ac.uk](mailto:JenkinsN6@cardiff.ac.uk) (N. Jenkins), [cswang@tju.edu.cn](mailto:cswang@tju.edu.cn) (C. Wang), [t.green@imperial.ac.uk](mailto:t.green@imperial.ac.uk) (T. Green).

approaches proposed to increase the reliability of existing radially operated networks, momentary interruptions still exist when a fault occurs [6].

Upgrading of distribution networks from their original radial structure to a normally closed loop configuration is attracting attentions [7,8]. A closed loop configuration is advantageous over a radial one because the load can be balanced between feeders resulting in better voltage profiles and improved reliability of power supply [7]. However, such loop configuration increases the risk of wide area failures because any single network fault can be propagated quickly over a wide area. Thus, more complicated and expensive protection schemes are required for an interconnected network configuration [8,9].

Power electronic devices installed in place of NOPs in a distribution network, namely ‘Soft’ Open Points (SOPs) have been proposed to combine the benefits of both radial and loop (mesh) operated network while avoiding the drawbacks of each [9]. Instead of simply opening/closing NOPs, SOPs control load transfer and regulate network voltage profile by flexibly controlling active/reactive power flow between adjacent feeders. Immediate fault isolation between interconnected feeders as well as fast supply restoration is also enabled using these devices. Therefore SOPs are able to improve distribution network operation as well as facilitate a large penetration of low carbon technologies into the distribution network.

Previous studies have advocated the benefits of SOPs for distribution network operation [9–11]. It has been shown in [9,10] that SOP is a desirable alternative to other voltage control strategies for supporting DG growth. The coordination of SOP with local energy storage to damp the transients caused by the large-capacity distributed photovoltaic installations was presented in [11]. These studies mainly focused on normal network-operating conditions.

The behavior of an SOP device – back-to-back VSCs – under abnormal network-operating conditions was analyzed in [12]. However, only the condition during a fault was considered. The control philosophy and performance of the SOP to support post-fault supply restoration have not been explored.

To fill this gap, two control modes were developed for the operation of a back-to-back VSCs based SOP. The operating principle of a back-to-back VSCs based SOP was investigated under both normal and abnormal network operating conditions. The performance of the SOP using the two control modes was analyzed under various network operating conditions. The importance of the soft cold load pickup and voltage synchronization process, which are essential for a smooth transition between control modes during the change of network operating conditions, was also investigated.

## 2. Back-to-back VSCs based Soft Open Point

Fig. 1a shows a two-feeder distribution network interconnected with a back-to-back VSCs based SOP. Two VSCs are located between the feeder endpoints and connected via a common dc link. The main circuit topology of the back-to-back VSCs is shown in Fig. 1b. It consists of a dc capacitor to provide an energy buffer and reduce dc side voltage ripple, two two-level three-phase insulated gate bipolar transistor (IGBT)-based VSC to generate voltage waveforms using pulse width modulation (PWM). Each VSC terminal is connected to a series filter whose inductance is represented by  $L$ . This inductance provides high-frequency harmonic attenuation, limits the rate of rise of short circuit current, and facilitates control of power flow. The line resistance and reactance between the filter and the feeder endpoint are neglected since the line between the filter and the feeder endpoint is short.

The back-to-back VSC is suitable for SOP operation due to the following characteristics:

- (1) *Flexible active and reactive power control.* Both VSCs build their own voltage waveforms with desired amplitude and phase angle. This allows a full control of active power flowing through the dc link as well as independent reactive power supply or absorption at both interface terminals. Such controllability enables SOP operation for normal network operating condition, which includes feeder load balancing, power loss reduction and voltage profile improvement.
- (2) *Instantaneous and independent voltage control.* The voltage waveform built by the VSCs can be controlled dynamically within milliseconds thus enabling transient control, e.g. dynamic Volt/VAR control and power oscillation damping [13]. In addition, the VSC can build its own voltage without the need of an active source at the receiving end. Hence cold load pick up for supply restoration is achievable using such device.
- (3) *Isolation of disturbances and faults.* Transient overvoltage and overcurrent of VSCs are able to be limited by control strategies [14], thus network disturbances or faults on one connected feeder can be isolated from the other side by VSCs.

Two control modes were defined to operate the back-to-back VSC based SOP under both normal and abnormal network operating conditions. The power flow control mode was used to (1) regulate both active and reactive power flow on the connected feeders under normal network-operating conditions and (2) isolate fault between the interconnected feeders when a fault occurs on one feeder. The supply restoration mode was used under post-fault supply restoration conditions to provide power supply for the isolated loads on one feeder through the other feeder.

### • Power flow control mode

A dual closed-loop current-controlled strategy [15] was used to operate SOP for the control of the feeder power flow under normal network operating conditions. Such current-controlled strategy is advantageous because: (1) it provides de-coupled control of active and reactive power components and (2) it inherently limits the VSC current during network faults.

Fig. 2 presents the overall control structure. The outer power control loop, the inner current control loop and the phase locked loop (PLL) are the three main components. In the outer power control loop (Fig. 2a), one of the VSCs operates with the  $P$ - $Q$  control scheme where the active and reactive power errors are transformed into the reference  $d$ - $q$  current components,  $i_d^*$  and  $i_q^*$  through the PI controllers. Superscript asterisk denotes the reference values. The other VSC operates with the  $V_{dc}$ - $Q$  control scheme maintaining a constant dc side voltage for a stable and balanced active power flowing through the dc link. Dynamic limiters for  $i_d^*$  and  $i_q^*$  are inserted to enable overcurrent limiting during network faults and disturbances. In the inner current control loop (Fig. 2b), the reference VSC  $d$ - $q$  voltage,  $V_{dm}$  and  $V_{qm}$  are determined through the PI controllers considering the  $d$ - $q$  current errors. The cross-coupling inductance  $L$  is the inductance between the VSC terminal and the feeder endpoint, i.e., the filter inductance as shown in Fig. 1b. This  $L$  remains constant when the power flow control mode is used for the operation of SOP. The voltage feed-forward and current feed-back compensations are used to get a good dynamic response [16]. After transforming  $V_{dm}$  and  $V_{qm}$  into the VSC terminal voltage by Park’s transformation [17], the gate signals for the IGBTs are obtained through the PWM. The PLL is important for the connection of VSCs to the ac network in order to synchronize the output VSC voltage with the ac network voltage. A PLL control topology based on the  $pq$  theory is used [18], as shown in Fig. 2c. By using the sum of the products of the feedback

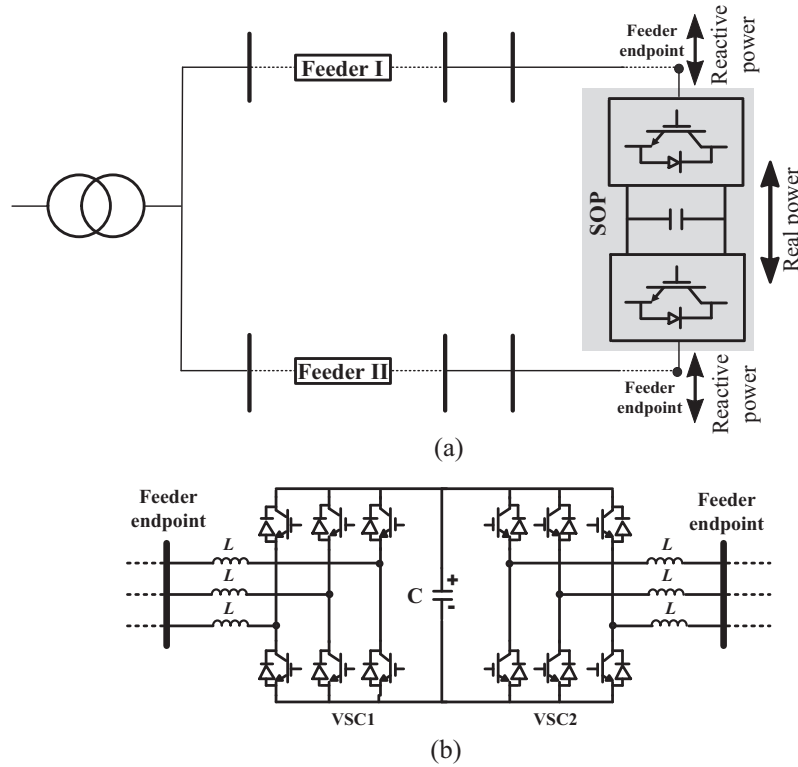


Fig. 1. (a) Basic configuration of a distribution network with an SOP; (b) main circuit topology of the back-to-back VSC based SOP.

signals,  $f_\alpha$  and  $f_\beta$ , and input  $\alpha$ - $\beta$  voltages transformed through Clark's transformation [17], the variation of the angular frequency  $\Delta\omega$  is calculated as

$$\Delta\omega = V_\alpha \cdot f_\beta + V_\beta \cdot f_\alpha \quad (1)$$

The PLL output angle  $\theta$  with a frequency  $f = 2\pi \cdot \omega$  is then obtained using a PI-controller, a feedback compensation of the base angular frequency  $\omega_b$  and an integrator.

• Supply restoration mode

When loads connected to one VSC of an SOP are isolated, the frequency and voltage of this VSC are no longer dictated by the grid. Using the previous current control strategy will cause voltage and/or frequency excursions that may lead to unacceptable operating conditions [19].

In such a case, the VSC connected to the isolated loads acts as a voltage source to provide a desired load voltage with stable frequency. The other VSC still acts as a current source operating with the  $V_{dc} - Q$  control scheme. Fig. 3 shows the block diagram of the voltage and frequency control strategy for the interface VSC. For voltage control, the VSC output voltage is controlled directly in the  $d$ - $q$  synchronous frame by holding  $V_q^*$  to zero and controlling  $V_d^*$  as

$$V_d = \sqrt{2/3} \cdot V_{rms}^* \quad (2)$$

where  $V_{rms}^*$  is the desired nominal line to line rms voltage of the isolated loads.  $\sqrt{2/3}$  is included because Park's transformation is based on the peak value of the phase voltage. The output VSC voltage is regulated by closed loop control and generated through the PWM scheme. Note that unlike the power flow control mode there is no cross-coupling inductance in the voltage control loop, which means that the voltage control strategy is not impacted by the value of the cross-coupling inductance. For frequency control, a stable

voltage frequency is generated by using the PLL. The input voltages of the PLL are assigned by transforming the same  $d$ - $q$  reference voltages for voltage control through Clarke's transformation. Thus,  $\Delta\omega$  in (1) is calculated as

$$\Delta\omega = V_d \cdot \cos \theta \cdot (-\sin \theta) + V_d \cdot \sin \theta \cdot \cos \theta = 0 \quad (3)$$

Since  $\Delta\omega$  remains zero, the phase angle  $\theta$  with a constant frequency  $f = 2\pi \cdot \omega_b$  is generated by integrating only the base angular frequency  $\omega_b$  as shown in Fig. 2.

3. SOP operation in MV distribution networks

The operating principle of the back-to-back VSCs based SOP under different network operating conditions and the performance of the SOP using the aforementioned two control modes were analyzed using a test system shown in Fig. 4. It consists of two MV feeders which are extracted from an IEEE 33-bus distribution network [19] and a back-to-back VSC based SOP placed between the feeders. This test system was modelled in EMTDC/PSCAD. The parameters of the SOP device are shown in Table 1. An average model was used to represent the SOP device, where losses, harmonics and fast switching transients of the converters were neglected [20,21].

3.1. Normal conditions

The feasibility of the control strategy for the power flow control mode was verified. Step changes on the active and reactive power reference signals were simulated. It is assumed that VSC1 is operated in  $V_{dc} - Q$  and VSC2 is operated in  $P - Q$  mode, as shown in Fig. 4. The reference step changes were simulated as follows: positive and negative step changes on VSC1 reactive power  $Q_1^*$  at 1 s and 2 s; on VSC2 reactive power  $Q_2^*$  at 1.5 s and 2.5 s and active power  $P_2^*$  at 1.5 s and 2 s; the dc side voltage  $V_{dc}^*$  remained a constant value.

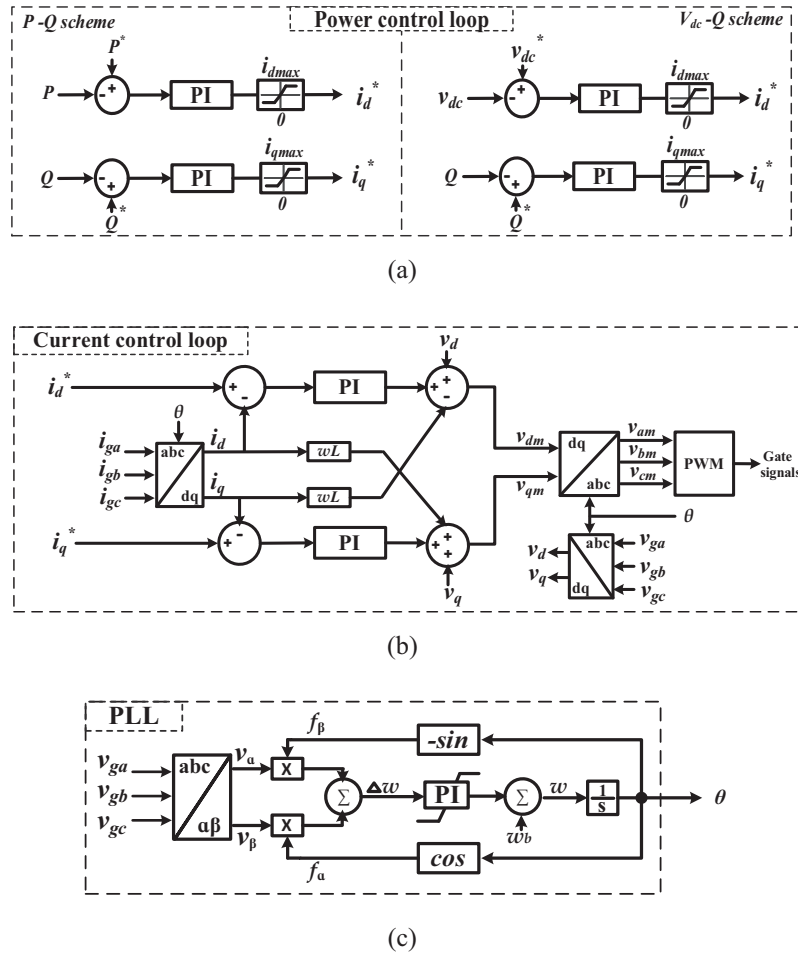


Fig. 2. Control block diagram of the SOP for power flow control mode.

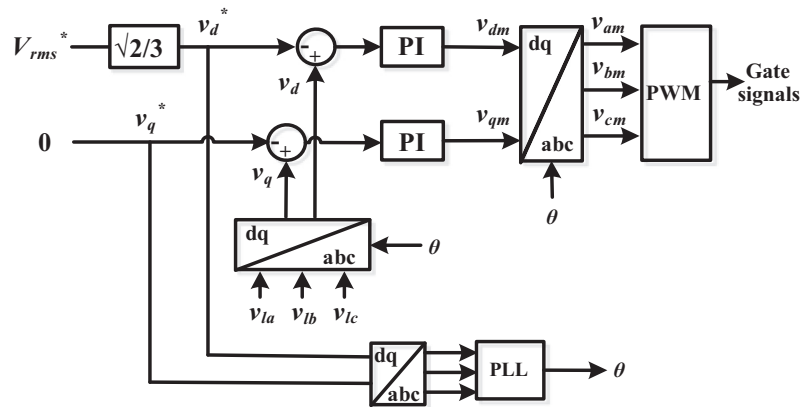


Fig. 3. Control block diagram of the interface VSC for the supply restoration control mode.

Fig. 5 shows the transient responses of the output power with respect to the step changes in reference signals. Good tracking performance was observed with an accurate and rapid steady condition attainment, i.e., within a few milliseconds without either an under damped response or overshoot. These results suggest the capability of the SOP to provide both instantaneous and longer duration power flow regulation as well as Volt/VAR control under normal network operating conditions. In addition, the dc link voltage remained a constant value except transient overshoots

occurring upon the step change on the active power, as shown in Fig. 5a. This is due to the sudden change of active power which caused instantaneous imbalance on active power exchange between the two feeders. Such undesired transient overshoots are usually damped by increasing the dc link capacitance. However, it is found that the extent of dc voltage overshoot reduced with the decrease of sudden change on active power. As shown in Fig. 5a, the dc voltage overshoot at  $t = 2$  s caused by a 0.5 MW power step change was much smaller than that at  $t = 1.5$  s upon

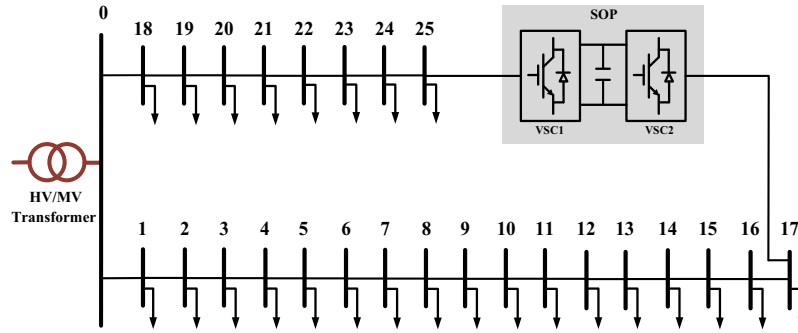


Fig. 4. Two-feeder MV distribution network with a back-to-back based SOP.

Table 1  
Parameters of the back-to-back VSC based SOP.

Parameters	Value
DC link voltage $V_{dc}$	35 kV
Filter inductor $L$	5 mH
DC link capacitor $C$	600 $\mu$ F
Rated power	1 MVA
Rated VSC voltage (line to line)	12.66 kV/50 Hz
Rated VSC current	0.08 kA

a 1 MW step change. This indicates that tuning the active power controller (PI controller) for a slower transient response is also viable to limit undesirable dc voltage overshoot without enlarging the dc capacitor.

### 3.2. During a fault

The behavior of the SOP device and its controllers (power flow control mode) was investigated under both balanced and unbalanced network faults. All simulations presented in this section

were conducted by assuming a fault occurs at Bus 13 (see Fig. 4). VSC1 is operated in  $V_{dc}$ -Q and VSC2 is operated in P-Q mode.

- *Balanced fault on the distribution network*

A three-phase fault was simulated at  $t = 1$  s with a fault impedance of  $3 \Omega$ . Such a high impedance fault was chosen to avoid triggering the internal protection of the SOP device that is typically designed to limit the VSC current to 2–3 times the full load current [22]. It was assumed that the fault is isolated by disabling the faulted side VSC after 200 ms. The active power (0.6 MW) flowing through the SOP from both direction was investigated.

Fig. 6 presents the simulation results including the voltage, current and power flow on both faulted and un-faulted side VSCs. Power was flowing from the un-faulted side feeder to the faulted side feeder before the fault occurred. As seen in Fig. 6a, the faulted side VSC had a limited contribution to the fault current before being disabled. The fault current became zero after the VSC was disabled. However, as expected its output voltage dropped to 2 kV (line to ground) and thus an under-voltage protection is sufficient to detect such a fault. In contrast to the faulted side VSC, the un-faulted side VSC had a regulated output current and voltage that were not affected by the fault, as shown

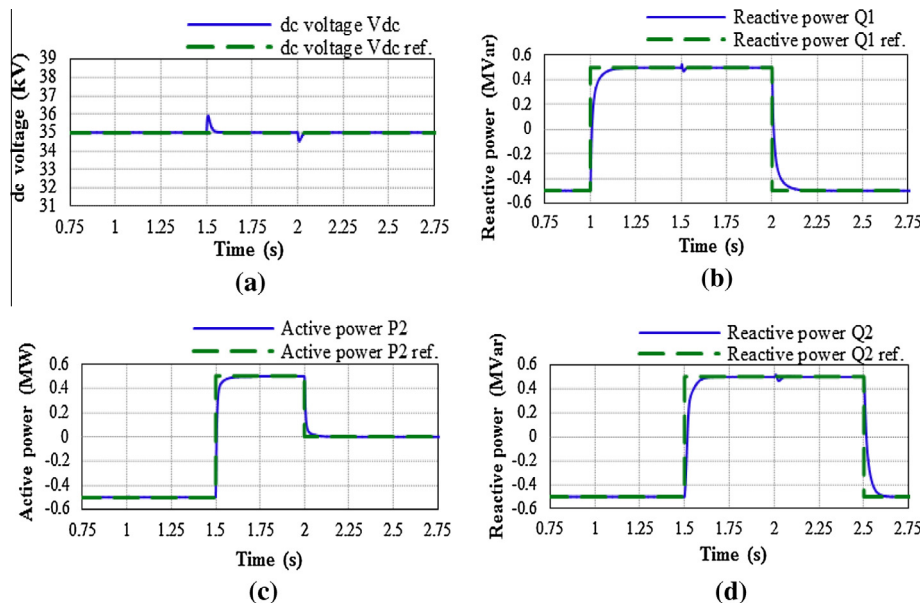
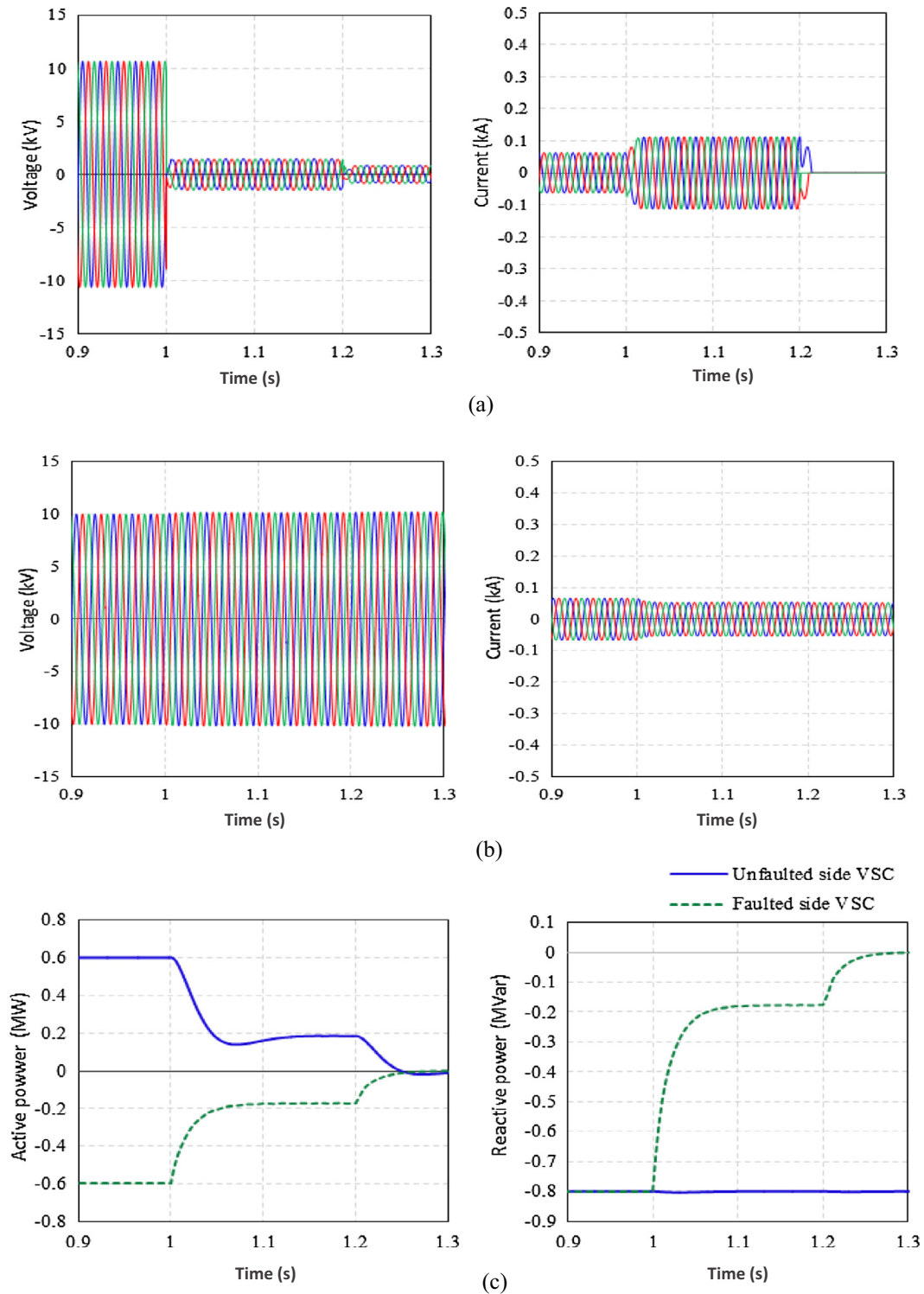


Fig. 5. Transient response of the power flow control mode to step changes in active and reactive power references: (a) dc side voltage; (b) reactive power response of VSC1; (c) active power response of VSC2; (d) reactive power response of VSC2.



**Fig. 6.** SOP response for a three-phase fault at  $t = 1$  s and isolated at  $t = 1.2$  s: (a) output voltage (left) and current (right) on the faulted side VSC; (b) output voltage (left) and current (right) on the un-faulted side VSC; (c) power flow on both VSCs.

in Fig. 6b. This suggests that the SOP device can effectively isolate a fault between the interconnected feeders. A reduction on the output current is observed after the fault occurred. This is due to the decrease of active power flow between the interconnected feeders.

Fig. 6c shows the real and reactive power flow of both VSCs. It is seen that both active and reactive power outputs on the faulted side VSC (dashed line) decreased during the fault, and then turned

to zero after disabling the faulted side VSC. Nevertheless, the reactive power output on the un-faulted side VSC (solid line) remained at the pre-fault value due to the de-coupled controllability of the control strategies.

When the pre-fault active power was flowing from the faulted side to the un-faulted side feeder, a similar SOP response as shown in Fig. 6 was observed which is not shown due to the space limitation.

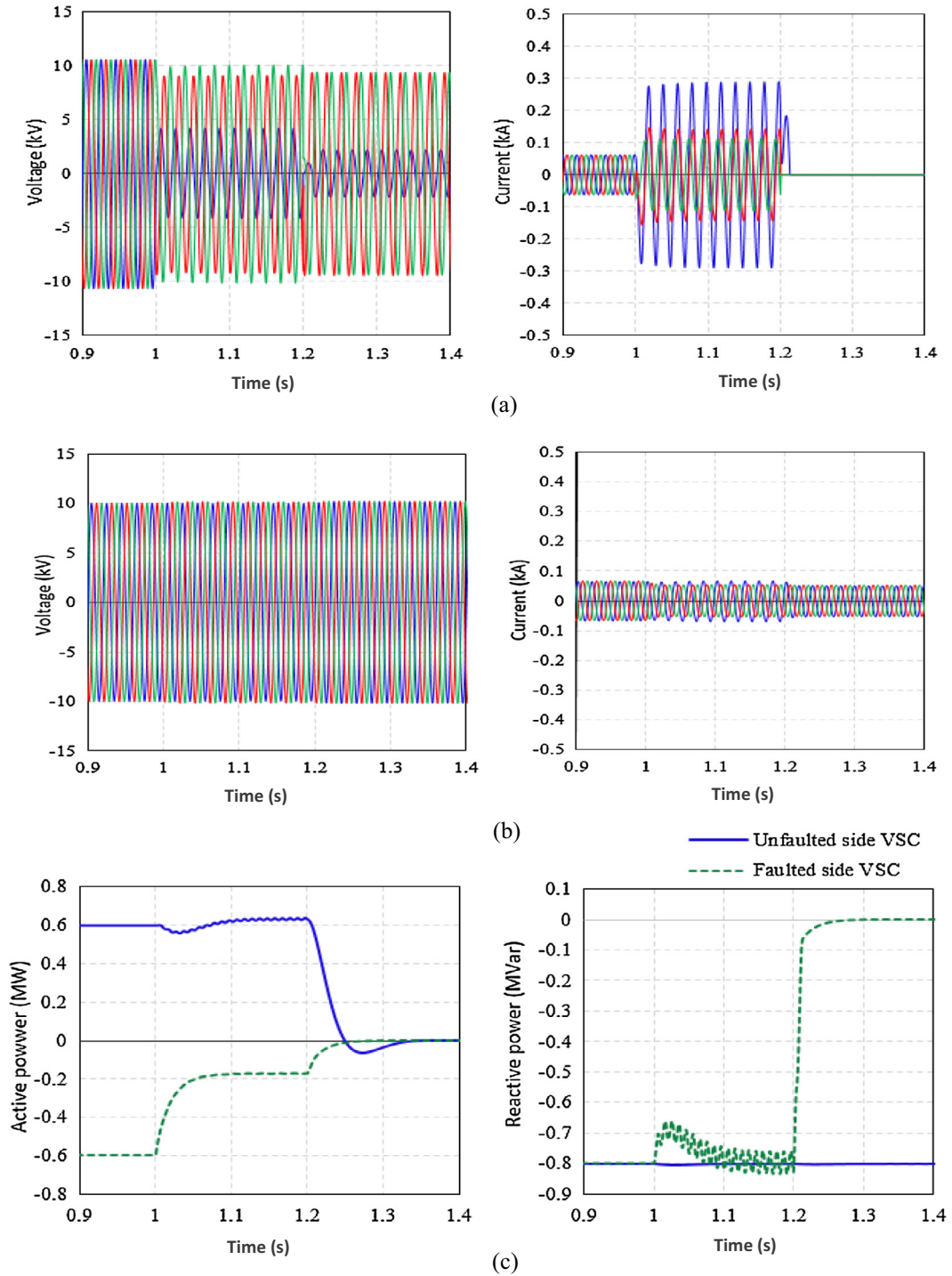


**Fig. 7.** SOP response for a single-phase to ground fault at  $t = 1$  s and isolated at  $t = 1.2$  s: (a) output voltage (left) and current (right) on the faulted side VSC; (b) output voltage (left) and current (right) on the un-faulted side VSC; (c) power flow behavior on both VSCs.

• *Unbalanced fault on the distribution network*

A single-phase to ground fault was simulated at  $t = 1$  s and isolated by disabling the faulted side VSC after 200 ms. The results are depicted in Fig. 7. It is observed that the faulted side VSC gave a greater contribution to the fault current compared to the balanced fault case, and thus may speed up the protection operation of the distribution network. Protection mechanisms based on negative sequence current and voltage are sufficient to protect feeders with

SOP for such a fault type. With respect to the un-faulted side VSC as shown in Fig. 7b, it can be seen that both output current and voltage remained at the pre-fault values despite the large fault current on the other side VSC.

Regarding the power flow, the output active and reactive power on the faulted side VSC remained at the pre-fault values but with notable ripple, as depicted in Fig. 7c. They became zero after the faulted side VSC was disabled. On the contrary, the reactive power supplied by the un-faulted side VSC was not affected by the fault,

which remained at the pre-fault value. When the pre-fault active power flows from the faulted side to the un-faulted side feeder, the SOP performance is similar to those shown in Fig. 7.

Simulations have also been conducted when the faulted side VSC operates using the  $V_{dc}$ - $Q$  scheme. Similar SOP performance was obtained to that shown in Figs. 6 and 7. From the results obtained, it is concluded that the SOP device and its controllers are effective in isolating fault between the connected feeders, thus limit the fault propagation on the network and the increase of short-circuit current. In addition, despite the occurrence of a fault, the reactive power controllability on the un-faulted side VSC remains.

### 3.3. Post-fault supply restoration conditions

Under this condition, the SOP is required to provide a smooth transition between different control modes: (1) from the power flow control mode to the supply restoration control mode to resume power supply to the un-faulted out-of-service loads; and (2) transfer back to the normal operation control mode when the isolated loads reconnect to the original feeder. Fig. 8 shows the transition system based on the control modes proposed in Section 2. The  $d$ - $q$  reference voltages input to the PWM modulation and the input voltages of the PLL controller are changed by two switches 'S<sub>1</sub>' and 'S<sub>2</sub>'. The controllability of the transition system under the post-fault supply restoration conditions was investigated. All simulations presented in this section follow the fault occurrence described in Section 3.2. The feeder terminal units (FTUs) were assumed to be installed in each branch and the total power of isolated loads were within the capacity of the SOP device. For a cold load pickup that exceeds the capacity of the SOP device, complicated implementation procedures, such as the coordination with the feeder automation has to be established, which is beyond the scope of this paper.

- *Transition from power flow control mode to supply restoration mode*

When a fault occurs at Bus 13, the fault is isolated by the network protection and the faulted side VSC is disabled. The SOP is changed to supply restoration mode to supply the un-faulted out-of-service loads, which is from Bus 14 to Bus 17. Once the supply restoration requirement is confirmed, switches 'S<sub>1</sub>' and 'S<sub>2</sub>' simultaneously change from the power flow control mode, 'PFC' to the supply restoration mode, 'SR'. It is assumed that the restoration requirement is confirmed at  $t = 2.2$  s, i.e., 1s after the

fault was isolated. This response delay represents the time used by the distribution automation to isolate a permanent fault and confirm the requirement of supply restoration.

Fig. 9 depicts the simulation results under a hard transition, i.e., directly connecting 'S<sub>1</sub>' and 'S<sub>2</sub>' to 'SR'. It is observed that when the output voltage waveform of the faulted side VSC was initiated from the desired reference value, a dc component was produced in the output ac current, as illustrated in Fig. 9b. This is due to the inductive isolated loads. In a highly inductive circuit, the instantaneous change on the applied voltage can lead to the dc component produced in order to maintain the initial current at zero [23]. As shown in Fig. 10a, such current dc offset became more severe when an inductance was connected in parallel with the isolated load (at Bus 17). Moreover, when a capacitance was connected in parallel with the isolated load (at Bus 17), a transient overshoot was also observed in the output current waveform, as shown in Fig. 10b. The capacitive loads such as power factor correction and voltage support capacitors connected to the distribution network are normally not automatically disconnected from the network during fault isolation. Both of these current dc offset and transient overshoots cannot be ignored due to the probability of triggering the inverter internal protection as well as the feeder protective relays.

A soft cold load pickup process to solve the current dc offset or inrush problems was proposed:

- (1) In order to avoid a sudden jump of the terminal voltage, at the instant of connecting switches 'S<sub>1</sub>' and 'S<sub>2</sub>' to 'SR', the initial values of both PLL angle and output voltage of the voltage controller are set to the values of the PLL angle and voltage magnitude just before switching to 'SR'.
- (2) The voltage controller (PI controller) is set for a slower transient response, i.e., a larger time constant to achieve a soft increase in the output voltage.

Fig. 11 shows the output voltage and current waveforms after using the soft cold load pickup process. It can be seen that the output voltage was increased smoothly without a sudden jump to the reference value. Either dc component or transient overshoot in the output current was successfully removed.

- *Transition from supply restoration mode to power flow control mode*

After the fault clearance, the isolated loads supplied by the SOP are reconnected to the original feeder. The SOP has to be changed from the supply restoration mode to the power flow control mode

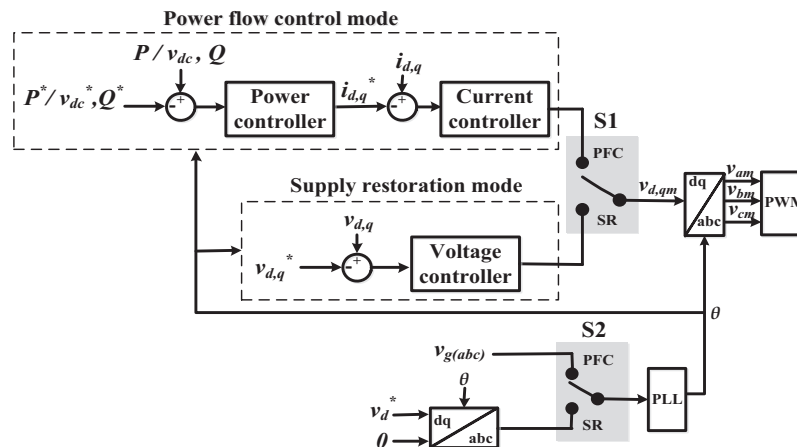


Fig. 8. Control mode transition system.

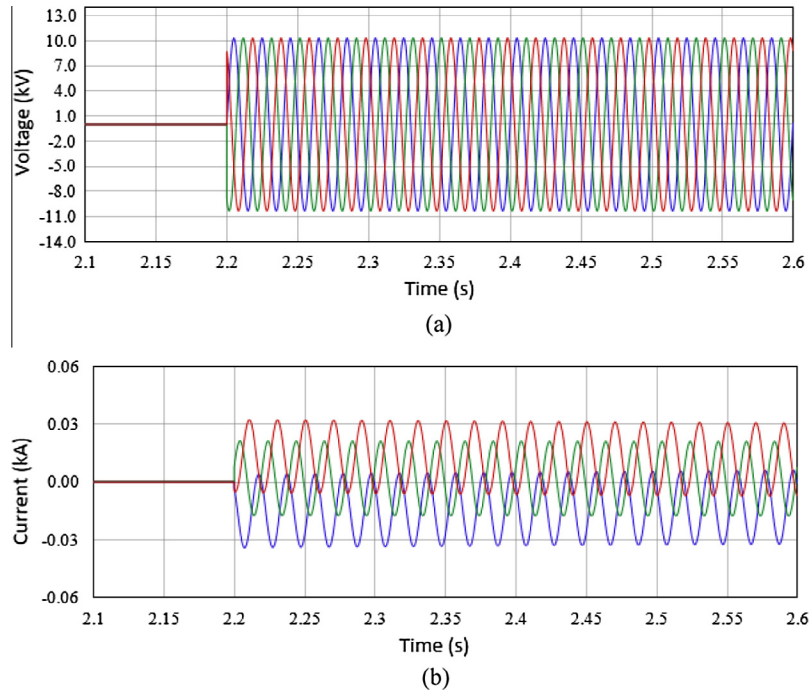


Fig. 9. Results of a hard transition to supply restoration mode at  $t = 2.2$  s: (a) output voltage waveform of the faulted side VSC; (b) output current waveform.

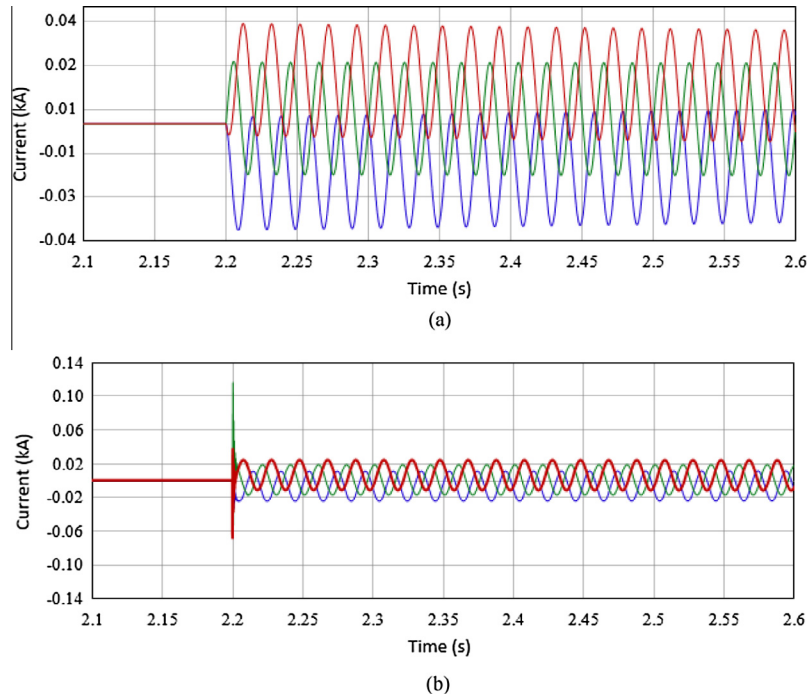


Fig. 10. Output current waveforms of the faulted side VSC for a hard transition when: (a) an inductance connected to Bus 17; (b) a capacitance connected to Bus 17.

by switching ‘ $S_1$ ’ and ‘ $S_2$ ’. The reconnection was assumed to occur at  $t = 3$  s. Fig. 12 depicts the simulation results. There was a current spike and voltage sag upon the transition, which may result in unexpected operation of the protection relays.

The reconnection is carried out after both voltage phase angle and magnitude are synchronized with the original feeder in order to avoid excessive transients. The detailed procedure for a seamless transition from the supply restoration mode to the power flow control mode is illustrated as follows:

- (1) Confirm that reconnection is required after the network fault has been removed.
- (2) The phase of the load voltage,  $\angle v_{L,r}$  at the reconnection point, i.e., at Bus 14, is synchronized with that of the original feeder voltage at Bus 13,  $\angle v_{f,r}$ :
  - The phase difference between the original feeder and the reconnection point voltage is obtained by

$$\Delta\theta = \angle v_{f,r} - \angle v_{L,r} \tag{4}$$

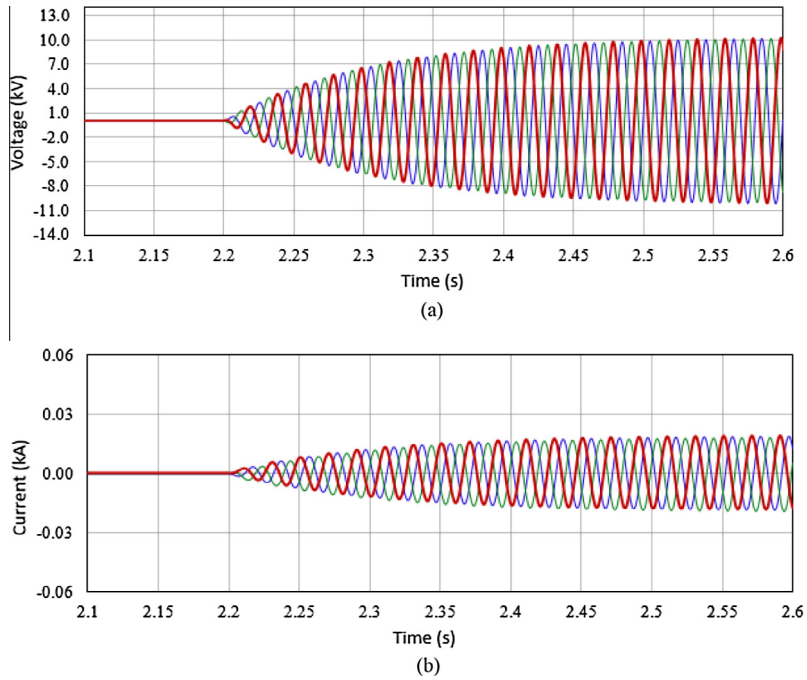


Fig. 11. Results of a smooth transition to supply restoration mode at  $t = 2.2$  s: (a) output voltage waveform of the faulted side VSC; (b) output current waveform.

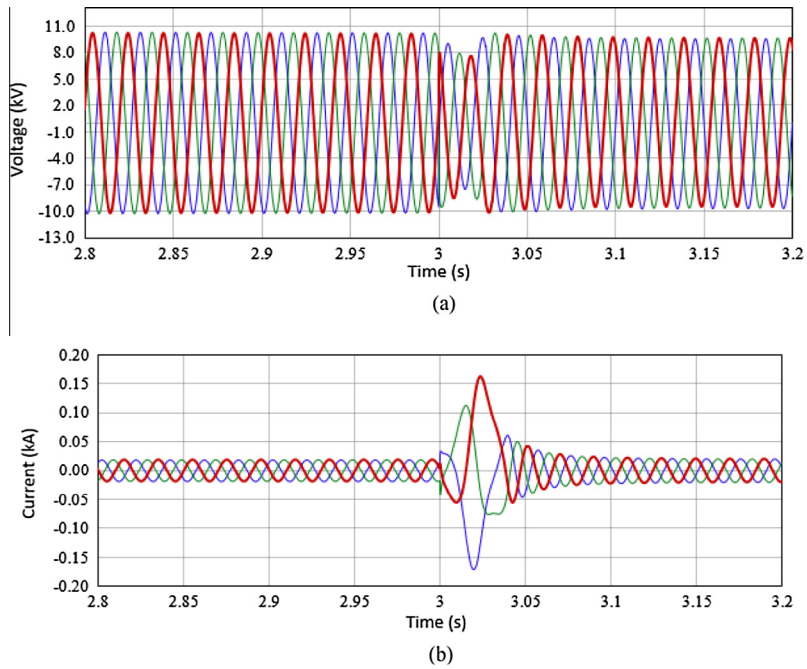


Fig. 12. Results of a hard transition to power flow control mode at  $t = 3$  s: (a) output voltage waveform of the faulted side VSC; (b) output current waveform.

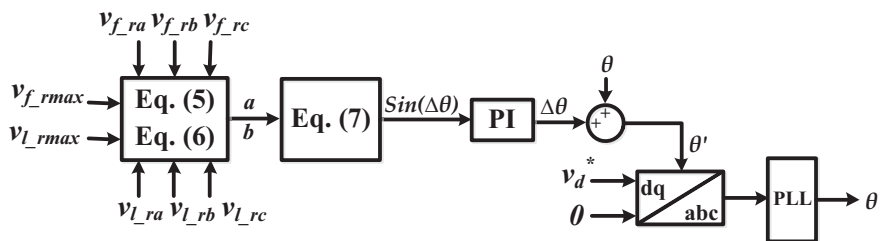


Fig. 13. Synchronization controller.

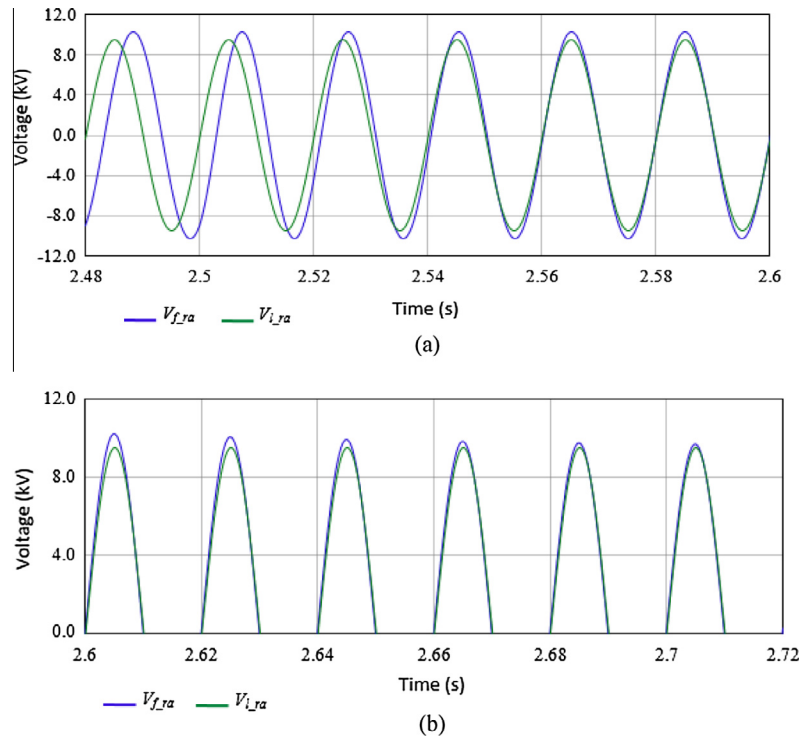


Fig. 14. Voltage synchronizations for reconnection: (a) phase synchronization; (b) magnitude synchronization.

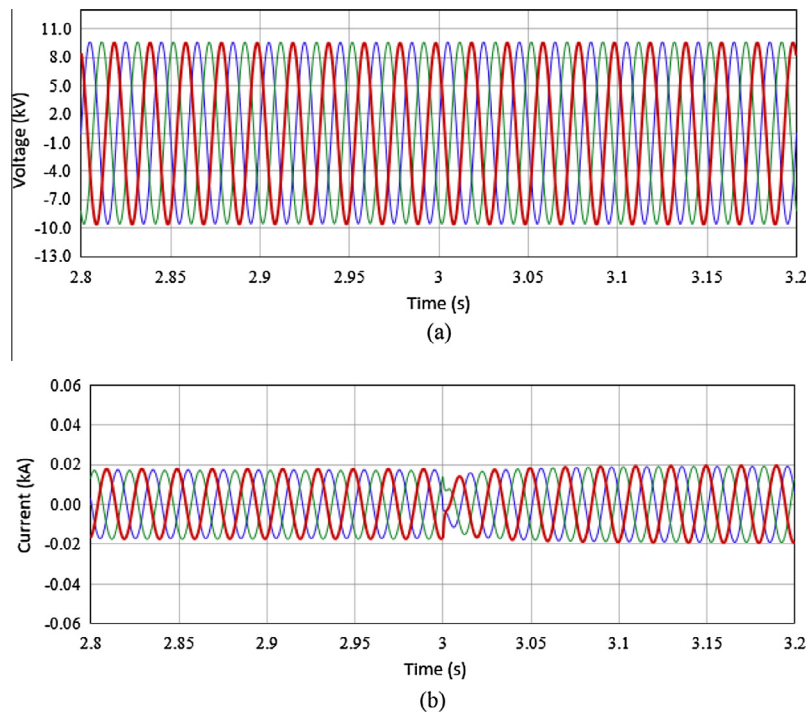


Fig. 15. Results of a smooth transition to power flow control mode at  $t = 3$  s: (a) output voltage waveform of the faulted side VSC; (b) output current waveform.

- Two sets of voltage values are used to obtain the information of  $\Delta\theta$

$$\begin{aligned} a &= v_{f\_ra} \cdot v_{l\_ra} + v_{f\_rb} \cdot v_{l\_rb} + v_{f\_rc} \cdot v_{l\_rc} \\ &= \frac{3}{2} \cdot v_{f\_max} \cdot v_{l\_max} \cos \Delta\theta \end{aligned} \quad (5)$$

$$\begin{aligned} b &= v_{l\_ra} \cdot v_{f\_rb} + v_{l\_rb} \cdot v_{f\_rc} + v_{l\_rc} \cdot v_{f\_ra} \\ &= \frac{3}{4} \cdot v_{f\_max} \cdot v_{l\_max} [-\cos \Delta\theta + \sqrt{3} \sin \Delta\theta] \end{aligned} \quad (6)$$

where  $v_{f\_ra}$ ,  $v_{f\_rb}$ ,  $v_{f\_rc}$  and  $v_{l\_ra}$ ,  $v_{l\_rb}$ ,  $v_{l\_rc}$  are the instantaneous phase voltages at Bus 14 and Bus 13,  $v_{f\_max}$  and  $v_{l\_max}$  are the maximum values of the instantaneous phase voltages at Bus 14 and Bus 13. More details for the deduction of Eqs. (5) and (6) are provided in Appendix A.

- Combining (5) and (6),  $\sin(\Delta\theta)$  is found as

$$\sin \Delta\theta = \frac{\sqrt{3}}{3 \cdot v_{f\_max} \cdot v_{l\_max}} \cdot \left( \frac{4}{3}b + \frac{2}{3}a \right) \quad (7)$$

Fig. 13 shows an overview of the phase synchronization process. 'S<sub>2</sub>' is switched to 'PFC' after the phase synchronization is completed.

- (3) The  $d$ - $q$  feeder voltages are assigned as the  $d$ - $q$  voltage references of the voltage controller in order to adjust the magnitude of the load voltage to that of the grid voltage.
- (4) When both phase and magnitude of the output voltage match the original feeder voltage, 'S<sub>1</sub>' is switched to 'PFC', and the isolated loads are reconnected to the original feeder. In order to prevent large transient flows of real and reactive power, the integrals of both power and current PI controllers are reset to zero and the reference values of real and reactive power are set as the value before transfer to the power flow control mode.

Fig. 14 shows the synchronization of the voltages when the synchronization algorithm started to work in the supply restoration mode. As can be seen, the synchronization process successfully forced the voltage at the end of the isolated area to track the voltage at the original feeder. Fig. 15 depicts the output voltage and current waveforms of the faulted side VSC after using the synchronization process. The current spike and voltage sag were successfully reduced.

A practical application of SOP in selected power distribution networks in the UK has been launched through the low carbon network fund (LCNF) [24]. The assessment on the performance of the back-to-back VSCs based SOP installed in Briton and London networks is being undertaken.

#### 4. Conclusion

Two control modes were developed for the operation of a back-to-back VSCs based SOP. For the power flow control mode, a dual closed-loop current-controlled strategy was used to regulate both active and reactive power on the connected feeders. For the supply restoration mode, a voltage and frequency control strategy was proposed to provide fast power supply restoration when the loads connected to one side of SOP are isolated due to network faults. The operational principle of the back-to-back VSCs based SOP was analyzed under both normal and abnormal network operating conditions. Case studies based on a two-feeder MV distribution network evaluated the performance of the SOP device using the

two control modes under normal, during a fault and post-fault supply restoration conditions.

Under normal conditions, the proposed SOP controller provides both instantaneous and longer duration power flow regulation between the interconnected feeders and the Volt/VAR support on both terminals. During fault conditions, the SOP controller (power flow control mode) is able to isolate either balanced or unbalanced network faults between interconnected feeders, and thus limit the fault propagation on the network and the increase of the short-circuit current.

Under post-fault supply restoration conditions, the SOP device was demonstrated to be effective in providing fast supply restoration through a seamless transition between the normal operation and the supply restoration modes. For the transition from the power flow control mode to the supply restoration mode, a soft cold load pickup process was preferred than the hard transition in order to remove the current dc offset and inrush problems which may trigger unexpected protection operations. For the transition from the supply restoration mode to the power flow control mode, the undesirable current overshoot and voltage lag were reduced after the use of the voltage synchronization procedure and the resets of current and power controllers.

#### Acknowledgements

This work was supported in part by the UK-China NSFC/EPSC OPEN project (Grant No. EP/K006274/1 and 51261130473) and the UK/India HEAPD project (Grant No. EP/K036211/1).

#### Appendix A. Deduction of Eqs. (5) and (6)

A balanced three-phase system is assumed and the instantaneous phase voltages at Bus 14 and Bus 13 are given by:

$$\begin{cases} v_{f\_ra} = v_{f\_max} \cdot \sin(\angle v_{f\_r}) \\ v_{f\_rb} = v_{f\_max} \cdot \sin(\angle v_{f\_r} - 120^\circ) \\ v_{f\_rc} = v_{f\_max} \cdot \sin(\angle v_{f\_r} + 120^\circ) \end{cases} \quad (A.1)$$

$$\begin{cases} v_{l\_ra} = v_{l\_max} \cdot \sin(\angle v_{l\_r}) \\ v_{l\_rb} = v_{l\_max} \cdot \sin(\angle v_{l\_r} - 120^\circ) \\ v_{l\_rc} = v_{l\_max} \cdot \sin(\angle v_{l\_r} + 120^\circ) \end{cases} \quad (A.2)$$

Substitute (A.1) and (A.2) into Eq. (5), thus

$$\begin{aligned} a &= v_{f\_ra} \cdot v_{l\_ra} + v_{f\_rb} \cdot v_{l\_rb} + v_{f\_rc} \cdot v_{l\_rc} \\ &= v_{f\_max} \cdot v_{l\_max} \cdot \sin(\angle v_{f\_r}) \cdot \sin(\omega t + \angle v_{l\_r}) + v_{f\_max} \cdot v_{l\_max} \cdot \sin(\angle v_{f\_r} - 120^\circ) \cdot \sin(\angle v_{l\_r} - 120^\circ) + v_{f\_max} \cdot v_{l\_max} \cdot \sin(\angle v_{f\_r} + 120^\circ) \cdot \sin(\angle v_{l\_r} + 120^\circ) \\ &= v_{f\_max} \cdot v_{l\_max} \cdot \left[ \frac{3}{2} \cdot \sin(\angle v_{f\_r}) \cdot \sin(\angle v_{l\_r}) + \frac{3}{2} \cos(\angle v_{f\_r}) \cdot \cos(\angle v_{l\_r}) \right] \\ &= \frac{3}{2} \cdot v_{f\_max} \cdot v_{l\_max} \cdot \cos(\angle v_{f\_r} - \angle v_{l\_r}) \\ &= \frac{3}{2} \cdot v_{f\_max} \cdot v_{l\_max} \cdot \cos \Delta\theta \end{aligned}$$

Eq. (6) is able to be deduced in a similar way.

#### References

- [1] Hung DQ, Mithulananthan N, Bansal RC. Integration of PV and BES units in commercial distribution systems considering energy loss and voltage stability. *Appl Energy* 2014;113:1162–70.
- [2] Mu Y, Wu J, Jenkins N, Jia H, Wang C. A spatial-temporal model for grid impact analysis of plug-in electric vehicles. *Appl Energy* 2014;114:456–65.
- [3] Abdullah MA, Agalgaonkar AP, Muttaqi KM. Assessment of energy supply and continuity of service in distribution network with renewable distributed generation. *Appl Energy* 2014;113:1015–26.
- [4] Fotouhi Ghazvini MA, Morais H, Vale Z. Coordination between mid-term maintenance outage decisions and short-term security-constrained scheduling in smart distribution systems. *Appl Energy* 2012;96:281–91.

- [5] Savić A, Đurišić Ž. Optimal sizing and location of SVC devices for improvement of voltage profile in distribution network with dispersed photovoltaic and wind power plants. *Appl Energy* 2014;134:114–24.
- [6] Lakervi E, Holmes EJ. *Electricity distribution network design*. 2nd ed. London (UK): Peregrinus; 1995.
- [7] Chen TH, Wei-Tzer H, Jyh-Cherng G, Guan-Chih P, Yen-Feng H, Tzong-Yih G. Feasibility study of upgrading primary feeders from radial and open-loop to normally closed-loop arrangement. *IEEE Trans Power Syst* 2004;19:1308–16.
- [8] Okada N, Kobayashi H, Takigawa K, Ichikawa M, Kurokawa K. Loop power flow control and voltage characteristics of distribution system for distributed generation including PV system. In: *Proceedings of 3rd world conference on photovoltaic energy conversion*, vol. 3; 2003. p. 2284–87.
- [9] Bloemink JM, Green TC. Increasing distributed generation penetration using soft normally-open points. In: *IEEE power and energy society general meeting*; 2010. p. 1–8.
- [10] Bloemink JM, Green TC. Benefits of distribution-level power electronics for supporting distributed generation growth. *IEEE Trans Power Del* 2013;28:911–9.
- [11] Bloemink JM, Green TC. Increasing photovoltaic penetration with local energy storage and soft normally-open points. In: *IEEE power and energy society general meeting*; 2011. p. 1–8.
- [12] Simanjorang R, Miura Y, Ise T, Sugimoto S, Fujita H. Application of series type BTB converter for minimizing circulating current and balancing power transformers in loop distribution lines. In: *IEEE conference on power conversion*. Nagoya; 2007. p. 997–1004.
- [13] Trujillo CL, Velasco D, Guarnizo JG, Díaz N. Design and implementation of a VSC for interconnection with power grids, using the method of identification the system through state space for the calculation of controllers. *Appl Energy* 2011;88(9):3169–75.
- [14] Jacobson B, Jiang-Hafner Y, P. Rey GA, Jeroense M, Gustafsson A, Bergkvist M. HVDC with voltage source converters and extruded cables for up to  $\pm 300$  kV and 1000 MW. Cigre, Paris, France; 2006. p. B4–105 [1–8].
- [15] Chaudhuri NR, Majumder R, Chaudhuri B, Jiuping P. Stability analysis of VSC MTDC grids connected to multimachine AC systems. *IEEE Trans Power Del* 2011;26:2774–84.
- [16] Espi Huerta JM, Castello-Moreno J, Fischer JR, Garcia-Gil R. A synchronous reference frame robust predictive current control for three-phase grid-connected inverters. *IEEE Trans Ind Electron* 2010;57:954–62.
- [17] Balaguer IJ, Qin L, Shuitao Y, Supatti U, Fang Zheng P. Control for grid-connected and intentional islanding operations of distributed power generation. *IEEE Trans Ind Electron* 2011;58:147–57.
- [18] Rolim LGB, da Costa DR, Aredes M. Analysis and software implementation of a robust synchronizing PLL circuit based on the pq theory. *IEEE Trans Ind Electron* 2006;53:1919–26.
- [19] Fang G, Iravani MR. A control strategy for a distributed generation unit in grid-connected and autonomous modes of operation. *IEEE Trans Power Del* 2008;23:850–9.
- [20] Cole S, Beerten J, Belmans R. Generalized dynamic VSC MTDC model for power system stability studies. *IEEE Trans Power Syst* 2010;25:1655–62.
- [21] Silva B, Moreira CL, Leite H, Lopes JA. Control strategies for AC fault ride through in multiterminal HVDC Grids. *IEEE Trans Power Del* 2014;29:395–405.
- [22] Nikkhajoei H, Lasseter RH. Microgrid protection. *IEEE conference on power engineering society general meeting*; 2007. p. 1–6.
- [23] Stringer NT. The effect of DC offset on current-operated relays. *IEEE Trans Ind Appl* 1998;34:30–4.
- [24] UK Power Networks. Ofgem – LCNF Tier 2 project: Flexible Urban Networks Low Voltage. Available: <<http://innovation.ukpowernetworks.co.uk/innovation/en/Projects/tier-2-projects/Flexible-Urban-Networks-Low-Voltage/Project-Documents/Overview+Flexible+Urban+Networks+Low+Voltage+-+Jan+2014.pdf>>.